Proceedings of the ASME 2017 International Technical Conference and Exhibition on Packaging and Integration of Electronic and Photonic Microsystems
InterPACK2017
August 29-September 1, 2017, San Francisco, California, USA

IPACK2017-74148

Transient Thermal Performance of Rear Door Heat Exchanger in Local Contained Environment during Water Side Failure

Kourosh Nemati[1], Husam A. Alissa[2], Mohammad. I. Tradat[3], Bahgat Sammakia[3]
[1]Future Facilities, New York, NY, USA
[2]Microsoft, Redmond, WA, USA
[3]Departments of Mechanical Engineering, Binghamton University-SUNY, NY, USA
E-mail: kourosh.nemati@futurefacilities.com

Abstract

The constant increase in data center computational and processing requirements has led to increases in the IT equipment power demand and cooling challenges of high-density (HD) data centers. As a solution to this, the hybrid and liquid systems are widely used as part of HD data centers thermal management solutions.

This study presents an experimental based investigation and analysis of the transient thermal performance of a stand-alone server cabinet. The total heat load of the cabinet is controllable remotely and a rear door heat exchanger is attached with controllable water flow rate. The cooling performances of two different failure scenarios are investigated. One is in the water chiller and another is in the water pump for the Rear Door Heat eXchanger (RDHX). In addition, the study reports the impact of each scenario on the IT equipment thermal response and on the cabinet outlet temperature using a mobile temperature and velocity mesh (MTVM) experimental tool. Furthermore, this study also addresses and characterizes the heat exchanger cooling performance during both scenarios.

1. Introduction

The objective of using hybrid and liquid cooling systems is to thermally management of high density data centers and improve energy efficiency while maintaining equipment reliability, as mentioned in [1,2]. The function of various types of Hybrid Cooling Systems is to bring the cooling source in proximity to the source of heat, with the goal of reducing room overcooling and hotspots while improving overall energy efficiency.

Hybrid cooling systems can be implemented as a stand-alone source of cooling or they can be used jointly with perimeter cooling systems. They even can be used as a self-contained unit for which an air liquid heat exchanger is mounted within a server cabinet such as a sidecar. This was introduced by IBM and is designed to remove up to 35KW as in [3]. A fully enclosed server cabinet, which employs a V-shape heat exchanger located on the bottom of the cabinet, is another type of self-contained hybrid cooling solution as reported by [4]. The authors showed that an uneven pressure balance in rack level containment could result in a higher equipment inlet air temperature. There are two important results from this study. First, sealing the leakage in the case of under provisioned airflow was followed by a significant decrease in the IT inlet air temperature. Second, mitigating leakage was more effective for cooling than reducing temperature. One of the most broadly used hybrid cooling system is a Rear Door Heat eXchanger. RDHX is mounted at the rear side of the cabinet where the hot exhaust air leaves the servers. There are many benefits to using RDHX in different data center configuration as shown in [5]. These benefits include: 1) reducing the number of Computer Room Air Handler (CRAH) units required. 2) Eliminating hot spots by removing more heat closer to the source and 3) Enabling higher chilled water temperatures while still maintaining IT inlet temperatures within the recommended ranges. Sundaralingam et al. [6] proposed a thermal approach that employed RDHXs in combination with room level air conditioning. The CRAC fan speed was optimized by a control system based on the heat load of the servers. This approach achieved an energy reduction of 47kWh, which was 6% of the total energy consumed by the Computer Room Air Conditioner (CRAC).

Preventing the cold and hot air streams from mixing is the main advantage of containment solutions. Various types of containment solutions can provide energy savings for both short and long-term usage. In [7] it was mentioned that 80% of current data centers are planning to install containment systems or are currently using them. Contained aisle solutions improve the uniformity of the air inlet temperature of IT equipment. thus, the supply air temperature of cooling units can be raised then compressor power consumption will decrease. Preventing recirculation is the main function of containment systems, but in some cases air leakage can take place from cold aisles to hot aisle or vice-versa. This is due to the difference in the air pressure distribution between the two aisles. The resulting air

leakage can significantly reduce the effectiveness of the containment on improving the desired efficiency.

Alissa et al. discussed the different types of cold and hot aisle leakage in [8]. They ranked and qualified the impact of leakage in terms of a Leakage Impact Factor (LIF) for different levels of airflow provisioning. They introduced a systematic approach on how to optimally employ containment systems in operational data centers. In [9] it was shown that under rack leakage is the most impactful source of leakage in cold aisles containment systems, and that airflow can be non-uniform through leakage paths. Patterson [10] investigated under rack leakage and monitored experimentally the temperatures near the bottom of the rack with infrared thermography. In [11], a new approach to characterize equipment was introduced. For this approach an effective flow curve is specified instead of the typical theoretical flow curve, the latter of which in some cases under estimates the required airflow. A flow bench used to generate flow curves of powered on servers. In [12], a steady thermal performance characterization of RDHX with a localized contained environment was experimentally investigated. The authors reported the effect of over and under-provisioning on the inlet temperature and air velocity uniformity. Their results showed a uniform inlet temperature combined with high air recirculation on the rack top in the case of over-provisioned. However, a back flow was observed near the top of the rack in the case of under-provisioning.

The main goal of this study is to investigate the thermal performance of an isolated server rack with a rear door heat exchanger in place during two waterside failure scenarios. A unique experimental facility has been developed in which air from a single perforated tile in front of the rack provides cooled air in addition to the RDHX. Pressure and airflow temperature are measured in the front and rear of the cabinet. A specialized mobile Temperature/Velocity Mesh (MTVM) measuring device was designed to experimentally map the temperature and velocity distribution in a vertical plane from the floor to the top of the rack. In addition, pressure /airflow relations for the equipment in the rack have been determined.

2. Experimental setup

2.1. Cabinet experimental setup

A uniquely designed experimental setup meant to improve the thermal analysis accuracy of the RDHX, placed in an DC lab which includes three cold aisles, as shown in Figure 1. A CW114DC1C Emerson Liebert (1930 mm Height x 3099 mm Width x 889 mm Depth) unit provides cold air through raised floor of the data center, which is called as the Energy-Smart Electronics Systems (ES2) lab at SUNY Binghamton [4]. The RDHX is setup on the top of the raised floor cutout with a single perforated tile. For the experiments reported here, the room temperature is kept between 24 °C (75.2 °F) and 26 °C (78.8 °F).

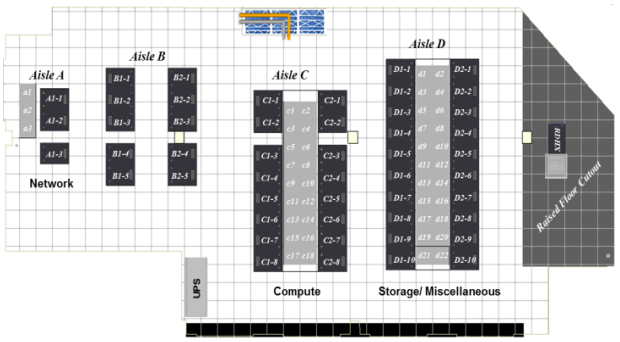

Figure 1. Data center laboratory layout

Figure 2a shows the RDHX attached to an IBM cabinet with a total IT capacity of 43 Rack Unit (RU). The rack IT load includes 16 DELL PowerEdge® 2950 servers (2RU). In addition, one 9RU load bank is located at the top of the cabinet. A stress load software program is used to vary the servers' stress loads to have variable power consumption. In the normal mode, each server dissipates about 235-265 W. In the full power mode, each generates about 390-420 W. The power of the load bank can be varied from 1 kW to 10.5 kW. The equipment in total can generate about 15.9kW. A master/slave arrangement 3 phase power distribution unit (PDU) is attached to the cabinet IT load (servers and load bank) to collect the dissipated power of each unit. Airflow requirements of the 2RU servers vary depends on the server fan speed. The range starts with 56 CFM at the minimum fan speed (7200 RPM) and reaches 98 CFM at the maximum rotational speed (13000 RPM), while each side of the load bank requires 486 CFM of airflow. Therefore, the total required airflow is 1868 CFM, assuming the minimum server fan speed. An additional backpressure caused by the RDHX at the cabinet rear results in a non-free delivery point of airflow even with an open cold aisle configuration. Similarities can be drawn from the added backpressure from the RDHX and the structural effects like cable arms.

The cold air required for the cabinet is provided by a single perforated tile located in front of the cabinet, as shown in Figure 2a. Two types of perforated tiles are used during the experiments. One has an openness ratio of 65% and directional scoops, which delivers up to 1910 CFM airflow. Moreover, another with 22% openness is used. In the cases that the load bank is powered on the tile with higher air flow delivery was employed and for the cases with LB powered off (and covered) the perforated tile with lower openness ratio was used. During all the scenarios, the air pressure differential of the containment is measured. Localized cold aisle containment is installed to improve the air inlet temperature uniformity of the IT equipment. The leakage between the containment and the top of the cabinet and the under rack leakage are the dominant sources of leakage (Figure 3). The best practice to measure the airflow provisioning is to measure the air pressure in the containment. Two pitot tubes are situated at the middle height of the rack (one inside and one outside of containment). A positive pressure differential between the cold aisle and the

room at the same height based on equation (1) indicates that the system is over-provisioned. In order to reduce airflow leakage, the system must be slightly over-provisioned. In this case, the pressure differential is kept between 1 Pa to 3 Pa initially, which is achieved by varying the ACU air flow for different perforated tiles.

(a) Experimental setup front view (b) Experimental setup rear view

Figure 2. RDHX Experimental Setup.

$$\Delta P = P_{cold\ aisle} - P_{room} \quad (1)$$

A flow hood (ADM-850L) is used to capture the tile airflow for both types of tiles used during different experimental scenarios (closed and open containment door).

(a) Experimental setup with containment front view (b) Experimental setup with containment side view

Figure 3. Containment Experimental Setup.

2.2. Water side controller system

The RDHX is an air to liquid, cross-flow fin-tube heat exchanger that is mounted on the back of the server rack. On the water side of the heat exchanger a controller system is installed, which is shown in Figure 4a. In this setup, there are two loops of water. One loop is between the controller and the RDHX (loop A) and the other is between the water chiller and the controller (loop B). The controller system contains a water pump that controls the water flow rate in the heat exchanger loop (loop A), which can be set from 2 GPM to 8.5 GPM. The water flow rate is measured by a vortex flow meter installed on the return side of loop A. Three temperature sensors measure the water supply/return temperatures of the RDHX and chilled water temperature. The supply water temperature set point can be varied. A three-way valve controls the mixture percentage of the chilled water of loops A and B, and the adjustable valve controls the water supply temperature.

Figure 4b shows the schematic RDHX control system web interface. The system can maintain the set point temperature by a smart control algorithm that manages the water pump and the three-way valve. If the water pump is set to operational, then the three-way valve can be set to operational as well due to the adjustment by the control algorithm. The flow rate and temperatures can be monitored. Data is collected at controlled time intervals in most of the experimental cases. The pump flow rate and supply water set point are fixed and the three-way valve is controlled by the smart controller system.

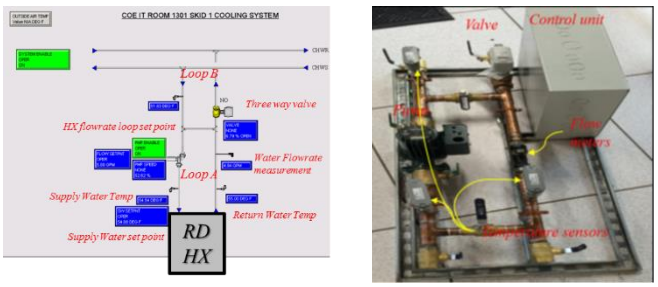

(a) Experimental water controller (b) Water controller schematic

Figure 4. Water controller system.

2.3. Mobile Temperature/Velocity Mesh (MTVM)

A Mobile Temperature /Velocity Mesh (Figure 5a) has been designed to measure the air temperature and velocity at the same time in front and behind the cabinet. The temperature/velocity mesh is installed on a mobile aluminum frame. The AccuSense™UAS1000 [14] sensors in array of three by twelve (3 horizontal by 12 vertical) is installed on the mesh. UAS1000 measures the air velocity and airflow temperature simultaneously. The velocity sensors are full range hot wires, 0.15 m/s to 20 m/s (30-4000 fpm), with an accuracy of ~5% of reading or ~0.05 m/s (10fpm). The temperature sensors are in a range of 0 - 70 °C (32-158 °F) with a measurement accuracy of ~1 °C (~1.8 °F). All 36 sensors are

attached to an ATM2400 data acquisition hub via USB ports. Robustness, light weight, air flow disturbance, and mobility are the factors used to design the MTVM. The frame consists of aluminum rails with L and T shaped brackets at the joints for rigidity to prevent vibration. Casters are attached under the frame for mobility. To help minimize air flow interference, the frame base is made the same size of a typical perforated tile (2 ft by 2 ft) such that it stands on the solid borders of the perforated tiles (Figure 5b). The temperature/velocity sensors are attached to a wire mesh located on one vertical side of the frame (Figure 5c). The sensors connect to a USB hub that is connected to a network switch. Data acquisition time intervals can be varied between 0.1 seconds to 10 hours. The sensor grid data is used to produce temperature/velocity contours using the MATLAB software environment.

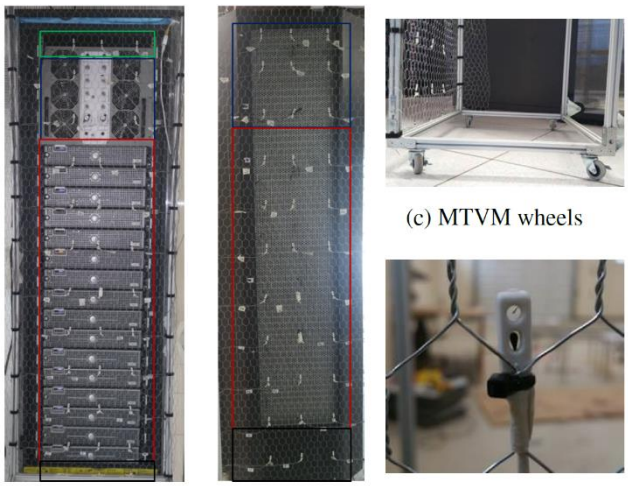

Figure 5. Mobile Temperature/Velocity Mesh (MTVM)

3. Failure scenarios description

Two different waterside failure scenarios in which the chiller or water pump of the RDHX fails are investigated. The primary focus is on the RDHX thermal behavior, including the outlet temperature and the cooling performance of the heat exchanger.

3.1. Chiller Failure - full power

Starting from an initial operational steady state, the chiller failure is simulated and the air and water temperatures are monitored until the system reaches the second steady-state. The second steady-state is indicated by the outlet temperature of the rack, which is monitored by the MTVM. Following this, the chilled water is restored and recovery takes place until the system reaches the third steady-state, which is very similar to the initial steady-state. To simulate the chiller failure, the three-way valve, which controls the mixture of fresh chilled water and water that is circulating in loop A, is closed. The valve is returned to automatic mode for recovery. The water temperature in loop A increases until all of the water circulating in loop A reaches the same temperature as the average outlet temperature of the IT (water supply and return temperatures become the same value). The heat capacities of the heat exchanger and water are important factors in this scenario, but the thermal inertia of the servers (and server simulator) do not play a role since the inlet air temperature and IT power generation are constant. In other words, conditions at the locations of planes 1 and 2 are not affected, while the conditions at plane 3 indicate the impact of the failure. For a data center, this scenario means losing the ability to chill water, while the circulating pump and the perimeter cooling system continue to function normally. In this case, the return air temperature of the CRAH is directly affected by this failure. It is assumed that the CRAH unit can always maintain the supply air temperature even during failure.

3.2. Chiller failure – half power

The presented failure scenario has non-uniform power generation and non-uniform air flow rate. In this section the same failure procedure will be carried out with a uniform air flow rate and power generation. For this purpose, the server simulator is powered off and covered and the perforated tile is changed to 22% perforation to keep the containment pressure at 1Pa to 3Pa. The IT required air flow is reduced to 800 CFM in this case. On the water side all the proprieties are kept the same as in the previous scenario.

3.3. Water Pump Failure – full power

In data centers the chilled water required by the RDHX is controlled by cooling distribution units (CDUs). Each CDU can serve multiple RDHXs simultaneously. Based on the required cooling power, the water flow rate of each RDHX is controlled by its local three-way valve. The CDUs typically contain two circulating water pumps (for redundancy). The data center vendor can select the active pump, either pump #1 or pump #2, or automatic. Selecting “Auto” means the control system switches the active pump at the selected date and time. If pump #1 or pump #2 is selected, then that pump will be the primary pump and will switch over to the standby pump on a loss of water flow after a programmed time delay has elapsed [15A]. In this section, the water pump failure scenario is investigated. To that end, the water pump in the water control system is powered off, which means the water circulation in loop A is stopped. The thermal behavior of RDHX in this failure scenario is different when compared to that of the chiller failure scenario.

3.4. Water Pump Failure – half power

Similarly, for the water failure scenario the half power case is investigated. The results are compared and presented in section 4.4.

4. Results and discussions

4.1. Chiller failure – full power

Cabinet inlet air velocity contours are shown in Figure 6a. The contours are generated using interpolation based on the 36 velocity readings from the MTVM sensors and assuming zero velocity at boundaries. The interpolation method used is not triangulation-based and not affected by the deterioration of the interpolation surface near boundaries. The velocity contours at the inlet show higher air velocity in the upper region (in front of server simulator fans), which is due to the air flow rate of the server simulator being higher than that of the 2 RU servers. The high air velocity at the middle height is due to the underfloor scoop design of the type perforated tile used, which tends to direct more of the tile air flow to this height. Because of the single flow direction capability of the hot wires used, only the air velocity magnitude in the primary flow direction can be measured. The velocity contours in the front side include a significant noise, which is likely due to the presence of turbulent eddies.

In Figure 6b) the temperature contours at the inlet region indicate that the temperature is fairly uniform. The color bar range is between 15 °C and 30 °C. The average is 20.1 °C with a tolerance of ~2 °C over the entire height of the rack. The air velocity contours at the outlet of the rack are shown in Figure 6c. The velocity reading at slice 3 shows less noise. The physical structure of the RDHX causes a pressure impedance and acts as flow straightener. This in turn causes the air flow to be more spread out at the rear of the cabinet, as can be seen in the contour. The bottom region shows high air velocity, which is due to the pressure impedance of the perforated plate being lower than that of the HX.

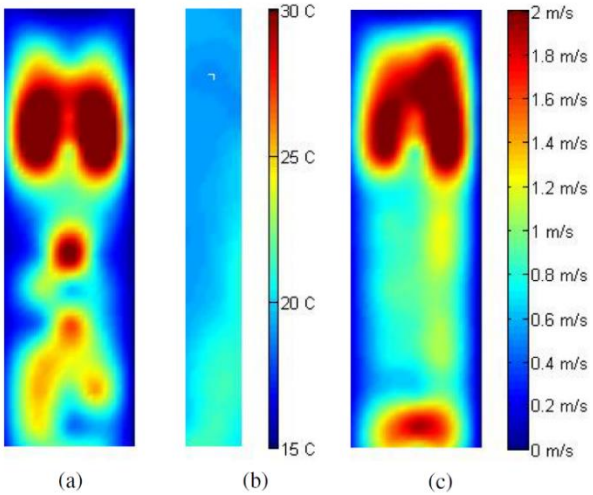

Figure 6. Inlet/outlet air temperature/velocity contours for Chiller failure-full power (a)&(b) At slice 1 (c) At slice 3

Figure 7 shows the outlet air temperature contours during the chiller failure. a) Figure 7a shows the temperature field at the initial steady-state. The upper region shows temperatures between 25.6 °C and 29.2 °C with a velocity weighted average of 27.3 °C. In the middle region the air temperature is between 18.6 °C and 22.3 °C with an average of 20.7 °C. The bottom region's average temperature is 33.5 °C. b) The water side failure happens at the moment shown in Figure 7b. It takes ~20 seconds until its effect can be seen with the air side temperature contours. The contour is basically the same as that of 7a since the system remains at a steady-state. c) Figure 7c takes place after 60 seconds of failure. The higher region of the HX heats up faster than the lower parts due to a higher air flow rate and outlet temperature of the LB. The bottom region temperature is constant since the server's boundary condition is constant. d) Figure 7d shows the half way state between the first and second steady-states. The upper region reaches steady-state faster than the middle region. e) Figure 7e shows when the system reaches a steady-state and the outlet air temperature of the whole rack becomes almost consistent (2.5 °C tolerance). The heating rate of the upper region and middle region is 0.021 °C/s and 0.028 °C/s, respectively. The upper region reaches the second local steady-state with a lower temperature range faster (325 s) than the middle region (415 s). The effectiveness number of the middle part is lower due to the lower air flow rate. The water temperature heats up faster in the middle region and slows down the heating rate of the upper part. f) As it is shown in Figure 7f, qualitatively speaking the cooling rate of the upper part of the HX is lower that the middle region.The cooling rate of the upper region is 0.075 °C/s, which is behind the server simulator. For the middle part, the cooling rate is 0.095 °C/s. The cooling rate of the HX increases from the top to the bottom. Finally, the air side temperature contours when the supply water reaches the third steady-state are shown g) in Figure 7g, Note that the water side reaches steady-state faster than the air side.

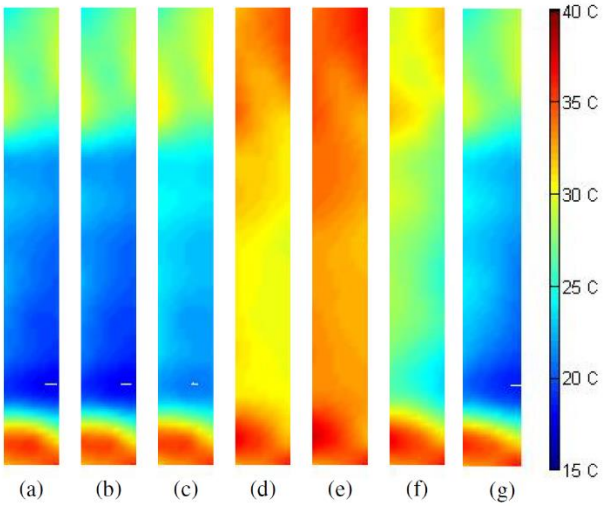

Figure 7. Outlet air temperature contour during chiller failure scenario-full power

For a more quantitative assessment, the average air side and water side inlet/outlet temperatures are shown in Figure 8. The plot begins at 15 seconds before the failure (in the first steady-state) and ends at 15 seconds after recovery (third steady-state).

The return water temperature (in red) becomes the same as the supply temperature since water only circulates in loop A. The water supply temperature (in blue) shows a sudden increase because the chiller fails (three-way valve closes). Initially, the supply temperature is the average of the chilled water temperature and the return temperature of loop A which depends on the three-way valve openness percentage. Once the chiller fails, this average increases to the return temperature within 40 seconds. The fluctuation of the supply water temperature that is observed during recovery can be attributed to the three-way valve ratio's justification to maintain the supply water set point. The supply water reaches the third steady-state within 105 seconds. The average inlet air temperature of the RDHX (in green) is constant since the failure is in the water side. The black dotted line is the average outlet air temperature of the RDHX in the upper region that is behind the load bank. It can be seen that the heating rate of the RDHX in this region is lower compared to that of the middle region (shown by the dashed line) and it reaches the second steady-state faster as well. During the second steady-state the dotted line shows temperature that is higher than the average inlet air temperature of the HX (in green), which is due to a number of sensors installed at the inlet of the upper region. The dashed line reaches the same temperature as the water temperature within 215 seconds of the failure. This means that the heat capacity of the HX structure delays the effect of failure on the air side for 215 seconds, but after that the water and air temperatures increase together. The black line is the velocity weighted average of the outlet air temperature of the HX. This temperature is different from the outlet temperature of the RDHX or the whole cabinet.

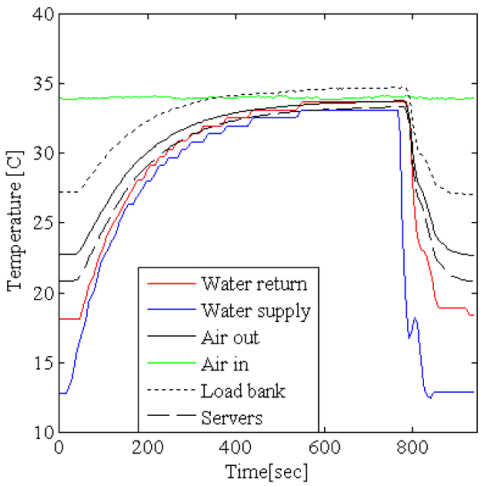

Figure 8. Inlet/Outlet air/water temperature during chiller failure scenario-full power

The inlet and outlet air temperatures of the load bank and four 2 RU servers (one on top, two in middle and one on bottom) have been measured and compared (shown in Figure 9a). The inlet temperature of the load bank and the servers shows a uniformity that is due to the contained cold aisle. Only server 16 (the bottom server) shows a temperature higher by 3 °C. This occurs because of under rack leakage, even though the system is slightly over-provisioned. Server 7 generates about 270Wand server 8 generates about 420 W. Since they have the same inlet air temperature and almost the same air flow rate, this difference in power generation makes the outlet temperature different by 3.5 °C. It can be concluded from the comparison of server 1 and 8 that while they generate the same amount of heat, server 1, which is closer to the LB, has a higher DT because of the lower air flow.

Figure 9b shows the transient effectiveness number of the HX. The effectiveness number is calculated based on the inlet/outlet air temperature and water supply temperature. It should be noted that since the air/water flow rates are constant, the air side always has a lower heat capacitance. Directly after failure the water temperature increases, but as it is shown in the temperature contours, the outlet air temperature is still constant. Since the inlet air temperature is always constant, the effectiveness value starts to increase. After 20 seconds, the average air temperature starts increasing, but the water temperature increase is still dominant. Within 110 seconds of failure, the air heating rate becomes dominant and the effectiveness value starts decreasing. After recovery, a sudden reduction of the effectiveness value is observed, which is due to the sudden decrease of the water supply temperature with a similar delay on the air side similar to the failure mode. Figure 9b also shows the three-way valve ratio,

which is at 26% initially. During the failure this percentage drops to zero and after recovery it fluctuates for 180 seconds until it reaches the third steady-state.

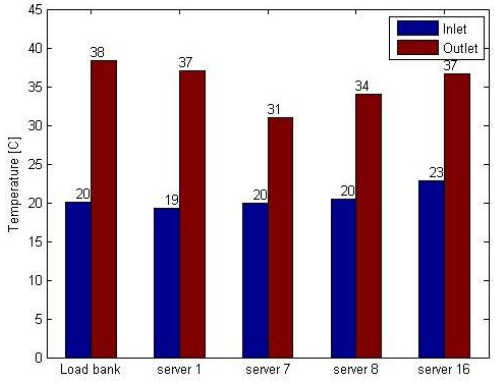

(a) Inlet/Outlet air temperature of IT

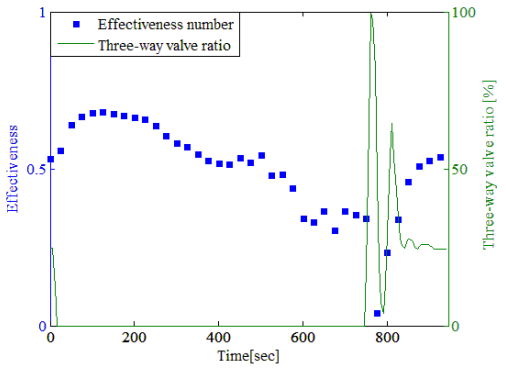

(b) Transient Effectiveness - Removed heat by water during failure

Figure 9. Chiller failure-full power

4.2. Chiller failure – half power

The velocity contours at slice 1 are shown in 10a. Since the flow rate is lower than that of the previous case, the air velocities are much lower as well. The upper region shows a very low air velocity (close to zero) and in front of the server a higher air velocity is observed (~0.4-0.8 m/s). However, the temperature contours in Figure 10b are similar to the full power case which shows uniformity. The outlet air velocity contour in Figure 10c shows an air velocity between 0.5 m/s and 0.7 m/s in the upper region, although the server simulator is powered off. The chamber between the server's outlet and the RDHX disperses the air flow. In another words, the additional pressure drop of the RDHX causes air recirculation in slice 2 of the cabinet. In the middle region a higher air velocity (close to 1 m/s) is observed on the right hand side just behind of the outlet of the servers, which is from where the majority of the servers air flow skips. The lower region of the velocity contours is comparable with that of the full power scenarios. Compared to the full power case, the air velocity at this region is much lower, which is due to the lower air recirculation in the cabinet, despite the air flow in the two bottom servers is the same. This shows that powering off the load bank significantly reduces the air pressure at slice 2.

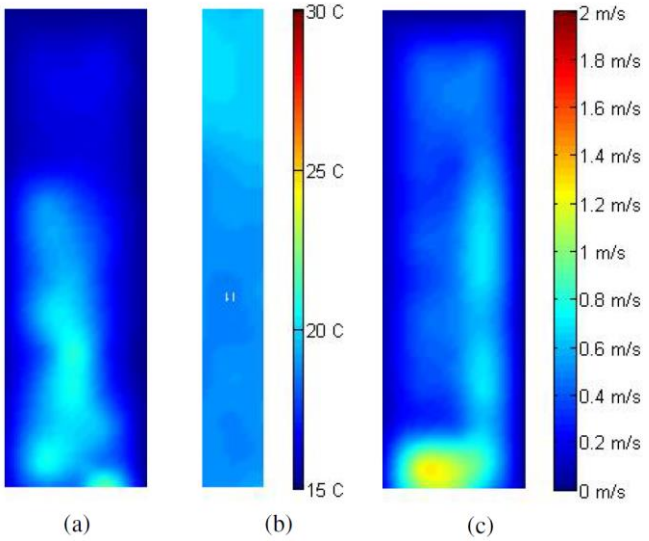

Figure 10: Inlet/outlet air temperature/velocity contours for Chiller failure-half power (a)&(b) At slice 1(c)At slice 3

The temperature contours are shown in the same order as in the previous failure scenario. a) & b) are in the first steady-state and when compared to the first scenario show about a 4.2 °C lower average. c) In the failure process it takes a longer time for the system to heat up and reach the second

steady-state. This is confirmed by the air temperature contours within 60 seconds of failure. The average air temperature increases by only 1.8 °C. In the previous case it is 2.9 °C. d) At the half-way point from the first to second steady-state the whole HX heats up at the same time. e) At the second steady-state the HX reaches approximately the same temperature as it does in the full power case. Since the exhaust temperature of the servers is constant in both cases, the outlet air temperature becomes the same for the middle region. Water circulation distributes the heat all over the HX and the same outlet air temperature is observed in the upper region. This provides a reason for why the same temperature is observed in Figure 11e all over the HX. f) The cooling rate of the HX is 0.064 °C/s for the upper region and 0.074 °C/s for the middle region. There is no heat load on the upper region, but the heat capacity of the HX is included while in the middle region, in addition to the HX thermal mass, the servers heat load is included as well. g) Compared to the full power case the system recovers slightly slower, although it should be noted that the heat load is about 60% lower.

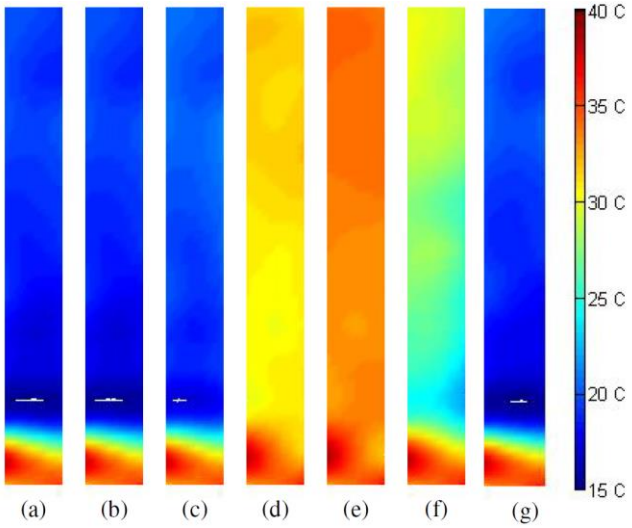

Figure 11: Outlet air temperature contour during chiller failure
scenario-half power

Figure 12 shows the air side and water side inlet/outlet temperatures during the failure. The air outlet temperature of the upper region increases with the same slope as that of the middle region since there is no heat load. The air temperature only increases because of increasing the water temperature. The HX contains two manifolds, one for supply and the other for return, with a large diameter feed pipe that is attached to both the supply and return hoses. The water flow rate is splitinto 16 circuits. The manifolds provide enough connection points so that a matching number of supply and return heat exchanger lines can be attached. The manifolds must also match the capacity rating of the pumps and the loop heat exchangers. The RDHX contains 16 individual heat exchangers, which the HX fins are shared between them. In this case, the inlet water temperature of all 16 circuits is assumed to be the same, but their water flow rate can vary. This provides a reason for the uniform temperature increase during failure. During recovery,

the water supply temperature shows two small fluctuations, which similar to the full power case is due to three-way valve ratio fluctuation needed to maintain the defined water supply temperature.

The average inlet/outlet air temperatures of the four servers are shown in Figure 13a. Since the load bank is powered off and covered, the temperatures in its vicinity have been eliminated from the chart. The inlet temperatures of the servers are uniform, but the outlet temperatures vary. The top server (server 1) shows the highest DT , which is because it has a relatively lower air flow and higher back pressure than the other servers.

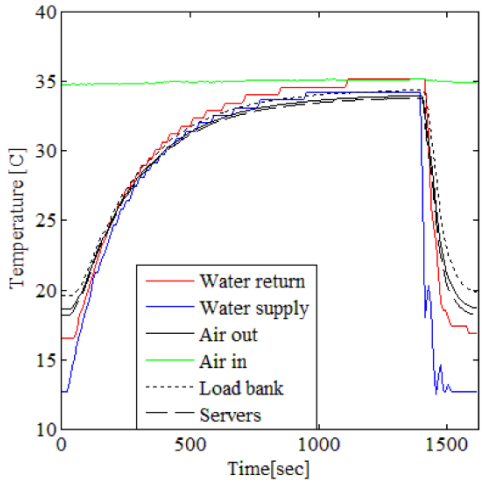

Figure 12: Inlet/Outlet air/water temperature during chiller failure scenario-half power

The effectiveness number shown in Figure 13b is calculated based on the steady-state effectiveness definition on the air side. The initial value is 0.71, but similar to the full power case, it increases after failure. The heat capacity of the RDHX material and the water in the loop A delays the air side temperature increase. Also, after 120 seconds of the failure the water in the loop and outlet air of the RDHX become the same, so the effectiveness number moves closer to 1. Closer to the second steady-state the effectiveness number reaches 1.4. At the second steady-state the value becomes 1.2. The reason for this reduction is that the air flow and the water flow rates are the same, but the cooling source was failed and the effectiveness approaches 1, which means the inlet/outlet air and inlet water temperature become the same. The three-way valve ratio that is shown in Figure 13b illustrates how the control system affects the ratio as it tries to keep the water temp set at 12.7 °C (55 °F).

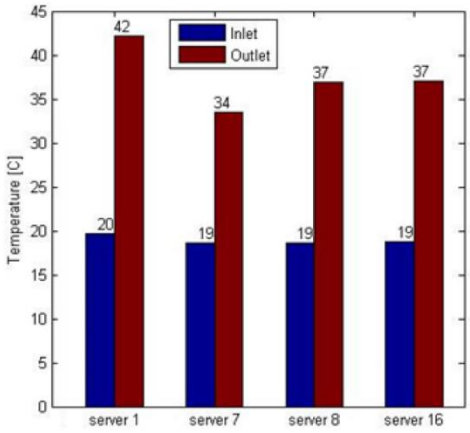

(a) Inlet/Outlet air temperature of IT

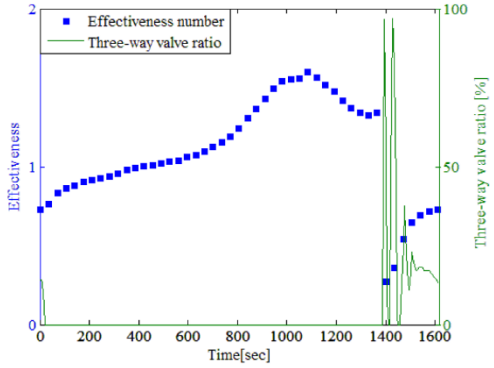

(b) Transient Effectiveness - Valve Ratio during failure

Figure 13: Chiller failure-half power

4.3. Water pump failure – full power

The thermal behavior of RDHX in this failure scenario is different when compared to that of the chiller failure scenario. In addition, the front side airflow rate and temperature are the same as those in the chiller failure scenario, which is because the perforated tile airflow, localized containment, and the servers are at the same conditions as well, as shown in Figure 14a & 14b. The constant airflow boundary condition results in the same air velocity contour for the rear side of the RDHX, as shown in Figure 14c. The initial boundary conditions of both the air and water-sides are the same for all failures.

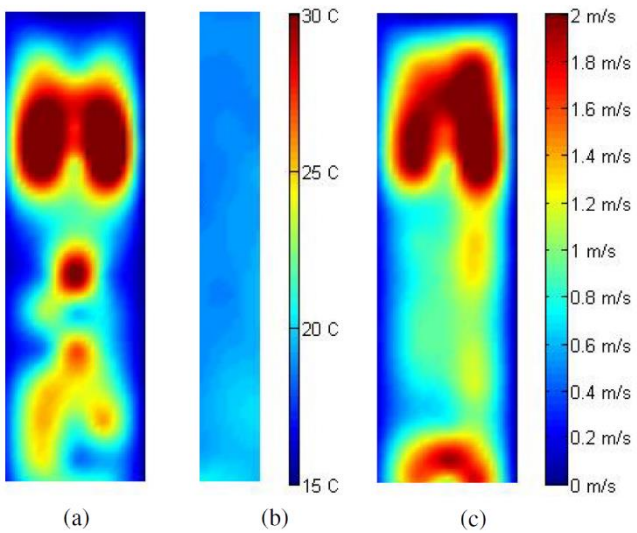

Figure 14: Inlet/outlet air temperature/velocity contours for Water pump failure-full power (a)&(b) At slice 1 (c) At slice 3

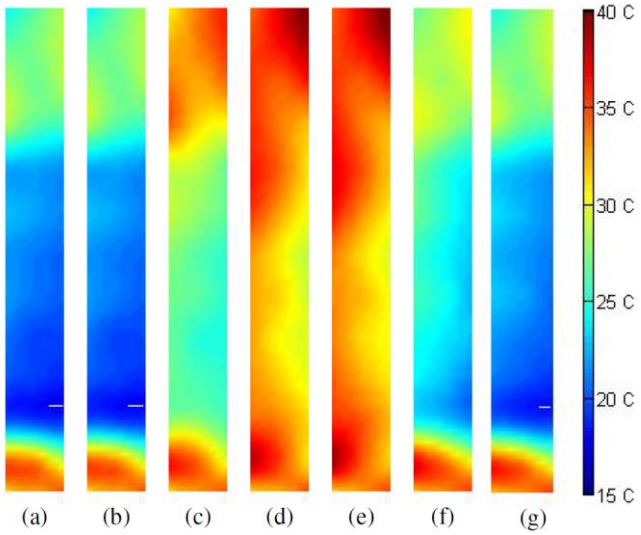

Figure 15: Outlet air temperature contour during water pump failure scenario-full power

The temperature contours at RDHX outlet during failure are shown in Figure 15. Similar to the chiller failure scenario, the temperature contours are taken at the first steady-state, shown in Figure 15a & 15b. When compared to the chiller failure, higher temperatures can be found within the 60 seconds after failure, as shown in Figure 15c, which means that the system is heating up faster in this case. There are two reasons for this time reduction. First, since the water circulation has stopped, the effectiveness number of the HX approaches zero. Second, the only portion of water that is trapped in the coil pipes heats up. In the other words, the trapped water's heat capacity is only effective on the outlet air temperature, which is almost half of the water that circulates in loop A. Figures 15d & 15e take place at the half way and full steady state failure, respectively. The temperature contours show less uniformity when compared to those of the chiller failure. In the chiller failure, the water circulation distributes heat over the HX. In the pump failure, temperature contours show high non-uniformity, similar to the non-uniformity seen in the power generation of the IT. Figure 15f & 15g are at the half way and full recovery steady-state, respectively. Similar to how the failure that is faster than the chiller failure, the recovery is faster as well. The water contained in the control system pipes and connection hoses remains at 12.7 °C during the failure (on the supply side). In this scenario, when the system recovers or the water starts to circulate, the inlet water is colder.

Figure 16 clearly shows that the average air temperature in the upper region (dotted line) is higher than the middle region of the HX (dashed line) during failure. However, the heating rate of the upper region is 0.06 °C/s and reaches steady-state faster due to a higher air flow rate. The heating rate of the middle region is 0.046 °C/s, while the overall rate is 0.048, which is closer to the middle region heating rate. On the water side of the HX, the water supply/return temperature is constant during failure since the water is trapped in the pipes. The only source of heating that is observed in the supply side is the free convection of the water inside the pipes. The sudden temperature jump during recovery is mainly due to the temperature difference of the water trapped in the control system and the HX pipes. Since the three-way valve is closed, the supply temperature reaches the third steady-state within 40 seconds.

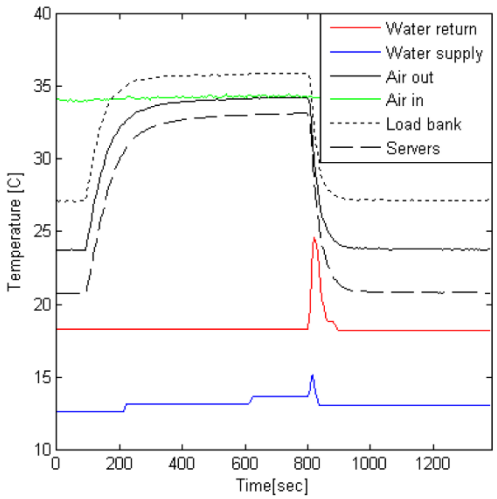

Figure 16: Inlet/Outlet air/water temperature during water

4.4. pump failure scenario-full power

Initially, the effectiveness number is 0.54 and it approaches zero since the water flow rate approaches zero, as shown in Figure 17. However, since the effectiveness number is calculated based on the steady-state effectiveness number definition at each time step and the transient term is not included, it takes 205 seconds for it to approach zero. While the supply air and water temperatures are constant, the effectiveness number is dependent on the variation of the air return temperature. The water side control system algorithm closes the three-way valve in special events like pump failure to prevent the mixture of the chiller water and water in loop A. As can be seen in Figure 17, this is the reason that during the failure the three-way valve goes to zero. The server inlet/outlet temperatures are not included in this section since they are similar to those found in the chiller failure scenario.

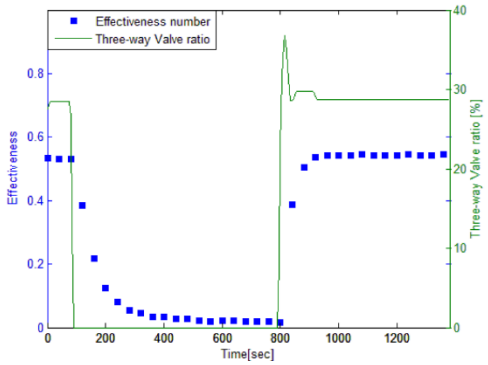

Figure 17: Transient Effectiveness - Valve Ratio during failure

4.5. Water Pump Failure - Half power

The outlet air temperature contours, which take place during the water pump failure with a half IT heat load, are shown in Figure 18. By comparing figures, it can be concluded that the heating rate of the pump failure is higher than that in the chiller failure. This goes for 11c and 18c for the half power cases as well. In the second steady-state, which is shown in Figure 18e, a higher air temperature is observed in the upper region even though the server simulator is powered off and covered. The distance between the outlet of the servers and the load bank to the RDHX (33cm and 43cm respectively) allows the hot air mixture to recirculate before entering the HX. The hot air with a higher air temperature moves upward and passes through the HX from the upper region. The temperature sensors that are installed at the inlet of the HX confirms this transition. However, Figure 18f, which takes place at the half-way during recovery, shows that the upper region recovers slower for the same reason.

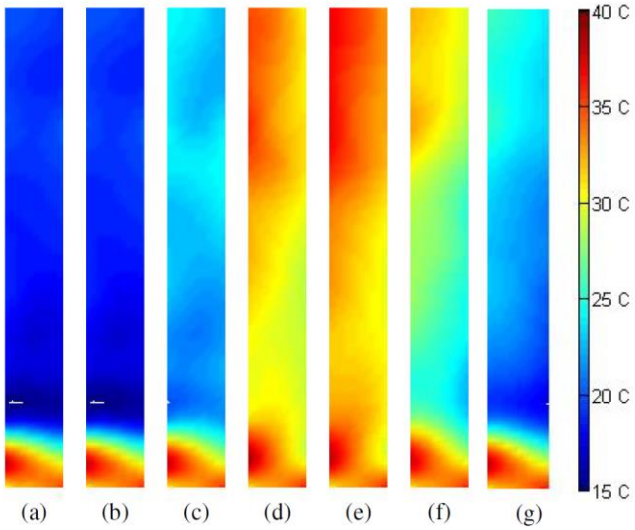

Figure 18: Outlet air temperature contour during water pump failure scenario-half power

The water supply/return temperature shows similar behavior to the full power case, shown in Figure 19). Initially, the air outlet temperature of the upper region is slightly higher than for the middle part, but during failure the difference is more significant, even more so than the average inlet temperature. Air with a higher temperature enters the HX through the upper region. The average outlet air temperature heating rate is 0.034 °C/s, while the cooling rate in the recovery mode is 0.052 °C/s.

The effectiveness number, which is 0.72 at the beginning of the experiment, approaches 0.1 during failure. Since the air flow rate is much lower than in the full power scenario and the water flow rate approaches zero, it takes a very long time for the system to reach the failure steady-state. If the system reaches the failure steady-state, then the effectiveness number must be zero. This also applies to the full power scenario, which has a higher air flow rate. This means that the inlet and outlet air temperature approach the same number. It should be noted that here the three-way valve has a performance similar to its one in the full power scenario.

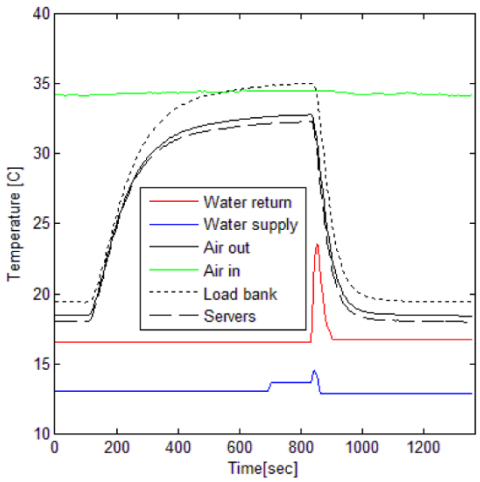

Figure 19: Inlet/Outlet air/water temperature during water pump failure scenario-half power

5. Conclusions

This paper includes an experimentally based analysis and investigation of transient thermal performance of a uniquely designed experimental setup. A rear door heat exchanger attached to an IBM cabinet which populated by 16 DellTMPowerEdgeTM2950 servers and a 9 RU load bank. Different types of instruments were used to measure airflow rate, pressure, velocity, humidity and temperature including MTVM which was used to develop a map of the cabinet inlet/outlet temperature and airflow distribution.

Two water sides failure scenarios of the RDHX involved in the current study to address the effect of supply water temperature on the RDHX performance. The main conclusions from the different aspects of the study are listed below:

1. Water chiller failure: In this case the mixture of chilled water and the water circulating in loop A was blocked by closing the three-way valve manually. For the recovery, the three-way valve control system was turned back to automatic mode.

(a) The water supply and return temperature increased to reach almost the same value as the average outlet air temperature.

(b) Since the water pump was still working the water circulation dispersed the heat and the outlet air temperature of the cabinet became almost uniform.

(c) The heating and cooling rate of the upper region was higher than the middle region in both the full and half power scenarios.

(d) The failure (system first steady-state to reach the second steady-state) and the recovery (second steady-state to reach the third steady-state) duration was higher in the half power case than in the full power case. This was due to lower air flow in the half power case. A higher air flow would increase the HX effectiveness.

(e) The 2 RU servers (”weaker IT”), which were closer to the server simulator (”stronger IT”), did not draw their required air flow. This was concluded from a comparison of the inlet and outlet air temperatures of different servers with similar power generation at different rack heights.

2. Water pump failure: Another water side failure was water pump failure. In this situation, the water pump was powered off and the water circulation in loop A was stopped. When the recovery took place the water pump went back to 60% (6GPM), similar to the initial state.

(a) This failure reached the second steady-state faster than in the chiller failure. This occurred because of the water thermal mass. In the chiller failure, the water temperature in loop A increased, but in the pump failure the temperature of the water trapped in the HX pipes increased. In other words, the water mass that absorbed heat was lower in the pump failure than in the chiller failure.

(b) Since the water flow was halted, the non-uniformity of the power generation of the IT equipment could be seen as a non-uniform air temperature at the outlet of the cabinet.

(c) The effectiveness number approached zero during the failure since the water flow rate was stopped. Given the thermal mass of the HX and trapped water, it took about 500 seconds for it to reach steady state (zero).

(d) The trapped water temperature in the control system and connection tubes was consistent during the failure, which enabled a faster recovery than in the chiller failure.

ACKNOWLEGMENTS

We acknowledge the support from the National Science Foundation under Grant 1134867. Also, we would like to acknowledge Kevin D. Hall from Binghamton University for his advice and help in conducting this experimental study.

References

[1] Airflow and Airflow Temperature Sensors for the ATM2400 Measurement System, The AccuSense, DegreeControl, Inc., User’s Guide.

[2] Jie Wei. Hybrid cooling technology for large-scale computing systems: from back to the future. In ASME 2011 Pacific Rim Technical Conference and Exhibition on Packaging and Integration of Electronic and Photonic Systems, pages 107–111. American Society of Mechanical Engineers, 2011.

[3] Roger Schmidt, Madhu Iyengar, Don Porter, GerryWeber, David Graybill, and James Steffes. Open side car heat exchanger that removes entire server heat load without any added fan power. In Thermal and Thermomechanical Phenomena in Electronic Systems (ITherm), 2010 12th IEEE Intersociety Conference on, pages 1–6. IEEE, 2010.

[4] Kourosh Nemati, Husam A Alissa, Bruce T Murray, Bahgat Sammakia, and Mark Seymour. Experimentally validated numerical model of a fully-enclosed hybrid cooled server cabinet. In ASME 2015 International Technical Conference

and Exhibition on Packaging and Integration of Electronic and Photonic Microsystems collocated with the ASME 2015 13th International Conference on Nanochannels, Microchannels, and Minichannels, pages V001T09A041–V001T09A041. American Society of Mechanical Engineers, 2015.

[5] Roger Schmidt and Madhusudan Iyengar. Server rack rear door heat exchanger and the new ASHRAE recommended environmental guidelines. In ASME 2009 InterPACK Conference collocated with the ASME 2009 Summer Heat Transfer Conference and the ASME 2009 3rd International Conference on Energy Sustainability, pages 851–862. American Society of Mechanical Engineers, 2009.

[6] Vikneshan Sundaralingam, Pramod Kumar, and Yogendra Joshi. Server heat load based crac fan controller paired with rear door heat exchanger. In ASME 2011 Pacific Rim Technical Conference and Exhibition on Packaging and Integration of Electronic and Photonic Systems, pages 489–496. American Society of Mechanical Engineers, 2011.

[7] S.K. Shrivastava, A.R. Calder, and M. Ibrahim. Quantitative comparison of air containment systems. In Thermal and Thermomechanical Phenomena in Electronic Systems (ITherm), 2012 13th IEEE Intersociety Conference on, pages 68–77, May 2012.

[8] H. Alissa, K. Nemati, B. Sammakia, K. Ghose, M. Seymour, D. King, and R. Tipton. Ranking and optimization of CAC and HAC leakage using pressure controlled models. In ASME 2015 International Mechanical Engineering Congress and Exposition. American Society of Mechanical Engineers, 2015.

[9] K. Nemati, T. Gao, B. T. Murray, and B. Sammakia. Experimental characterization of the rear door fans and heat exchanger of a fully-enclosed, hybrid-cooled server cabinet. In Semiconductor Thermal Measurement and Management Symposium (SEMI-THERM), 2014 30th Annual IEEE. IEEE, 2014.

[10] M. K. Patterson, R. Martin, J. B. von Oehsen, J. Pepin, Y. Joshi, V. K. Arghode, R. Steinbrecher, and J. King. A field investigation into the limits of high-density air-cooling. In ASME 2013 International Technical Conference and Exhibition on Packaging and Integration of Electronic and Photonic Microsystems, pages V002T09A013–V002T09A013. American Society of Mechanical Engineers, 2013.

[11] H.A. Alissa, K. Nemati, B.G. Sammakia, K. Schneebeli, R.R. Schmidt, and M.J. Seymour. Chip to facility ramifications of containment solution on it airflow and uptime. Components, Packaging and Manufacturing Technology, IEEE Transactions on, PP(99):1–12, 2016.

[12] K. Nemati and H. Alissa. Experimental Charcterization of a Rear Door Heat Exchanger with Localized Containment.

[13] Emerson Coolant Distribution Unit (CDU) Manual.

[14] *http://www.binghamton.edu/es2/.*